Rayleigh–Taylor shock waves

Britton J. Olson and Andrew W. Cook
Lawrence Livermore National Laboratory, Livermore, California 94551, USA

(Received 4 September 2007; accepted 30 October 2007; published online 28 December 2007)

Beginning from a state of hydrostatic equilibrium, in which a heavy gas rests atop a light gas in a constant gravitational field, Rayleigh–Taylor instability at the interface will launch a shock wave into the upper fluid. We have performed a series of large-eddy simulations which suggest that the rising bubbles of light fluid act like pistons, compressing the heavy fluid ahead of the fronts and generating shocklets. These shocklets coalesce in multidimensional fashion into a strong normal shock, which increases in strength as it propagates upwards. The simulations demonstrate that the shock Mach number increases faster in three dimensions than it does in two dimensions. The generation of shocks via Rayleigh–Taylor instability could play an important role in type Ia supernovae. © *2007 American Institute of Physics*. [DOI: 10.1063/1.2821907]

The quest to find a detonation mechanism for type Ia supernovae has spurred many investigations of Rayleigh–Taylor (R-T) unstable flame fronts.[1–8] However, the majority of R-T simulations and experiments to date have been performed in the incompressible or low Mach number regimes. Relatively little research has been performed on the effects of compressibility and hydrostatic density gradients on the late-time development of R-T turbulence. Mellado *et al.*[9] studied compressibility effects in R-T turbulence in an "unbounded" domain and concluded that "the Rayleigh–Taylor problem does not have significant intrinsic compressibility effects." Their research has reinforced the perception that R-T instability is a low Mach number phenomenon. The purpose of this brief communication is to demonstrate that R-T instability does in fact exhibit strong compressibility effects, as evidenced by the formation of shock waves in the upper fluid. The shock waves are observed when the flow domain is expanded beyond that of Mellado *et al.*

R-T instability between two ideal gases can be described by the following equations:

$$\frac{\partial \rho Y_i}{\partial t} + \nabla \cdot (\rho Y_i \mathbf{u} + \mathbf{J}_i) = 0, \quad i = 1,2, \tag{1}$$

$$\frac{\partial \rho \mathbf{u}}{\partial t} + \nabla \cdot [\rho \mathbf{u}\mathbf{u} + p\underline{\boldsymbol{\delta}} - \underline{\boldsymbol{\tau}}] = \rho \mathbf{g}, \tag{2}$$

$$\frac{\partial E}{\partial t} + \nabla \cdot [(E+p)\mathbf{u} - \underline{\boldsymbol{\tau}} \cdot \mathbf{u} + \mathbf{q}] = \rho \mathbf{g} \cdot \mathbf{u}, \tag{3}$$

$$p = \rho R T, \quad T = (\gamma - 1)e/R, \quad R = R_o \sum_{i=1}^{2} \frac{Y_i}{W_i}, \tag{4}$$

where ρ is density, Y_i is the mass fraction of species i, $\mathbf{u} = (u,v,w)$ is velocity, $\mathbf{J}_i$ is a diffusive mass flux, p is pressure, $\underline{\boldsymbol{\delta}}$ is the unit tensor, $\underline{\boldsymbol{\tau}}$ is the viscous stress tensor, $\mathbf{g} = (0,0,-g)$ is gravity, $E \equiv \rho(e + \mathbf{u}\cdot\mathbf{u}/2)$ is total energy (with e being internal energy), $\mathbf{q}$ is the heat conduction flux, γ is the ratio of specific heats (assumed to be the same for both gases), T is temperature, R is the apparent gas constant, R_o is the universal gas constant, and W_i is a species molecular weight. The viscous stress tensor is $\underline{\boldsymbol{\tau}} = \mu(2\underline{\mathbf{S}}) + (\beta - 2\mu/3) \times (\nabla \cdot \mathbf{u})\underline{\boldsymbol{\delta}}$, where μ is dynamic (shear) viscosity, β is bulk viscosity, and $\underline{\mathbf{S}}$ is the symmetric strain rate tensor, $\underline{\mathbf{S}} = [\nabla \mathbf{u} + (\nabla \mathbf{u})^{\dagger}]/2$, where $(\nabla \mathbf{u})^{\dagger}$ denotes the transpose of the dyadic $\nabla \mathbf{u}$. The conductive heat flux vector is described by Fourier's law, $\mathbf{q} = -\kappa \nabla T$, where κ is thermal conductivity. The diffusive (Fickian) mass fluxes are $\mathbf{J}_i = -\rho D \nabla Y_i$, where D is the diffusion coefficient. We solve Eqs. (1)–(4) using a tenth-order compact scheme for spatial derivatives, combined with a fourth-order Runge–Kutta integrator. In order to confine dissipation effects to the smallest possible scales, grid-dependent models are employed for μ, β, κ, and D. Complete details of the numerical method and subgrid-scale models, including verification and validation tests, have previously been presented.[10]

In our large-eddy simulations (LES) of R-T instability, xenon serves as the upper (heavy) fluid and krypton, argon or neon serves as the lower (light) fluid. The initial mass fractions are prescribed using a hyperbolic tangent profile in z, with a Gaussian spectrum of perturbations imposed at the interface.[11] The flows are initialized with isothermal fluids in hydrostatic equilibrium, i.e., we solve $dp/dz = -\rho g$, together with Eq. (4), to obtain p and ρ. In all simulations, gravity is $g = 980\ \mathrm{cm/s^2}$, the initial temperature is $T_0 = 300$ K, and the initial pressure at the top of the domain is $p_0 = 10^6$ Ba. The boundary conditions are periodic in x and y with slip walls on the top and bottom z boundaries. As a test of the hydrostatic initialization and wall boundary conditions, a few simulations were conducted with no perturbations to confirm that the flow remains undisturbed.

Figure 1 depicts a time sequence of the local Mach number from a 2D LES with neon used for the light fluid. The local Mach number is defined as $M_l(\mathbf{x},t) \equiv \|\mathbf{u}\|/c$, where $c = \sqrt{\gamma RT}$ is the local speed of sound. In the first image, the mixing region is clearly visible, with hints of acoustic waves just above the bubbles. In the second image, compression waves are seen emanating from the bubbles and coalescing further up in the xenon. In the third image, curved shocklets are apparent above the mixing region and a main shock has formed at higher elevation. In the fourth image, the post-shock Mach number has surpassed the maximum Mach num-

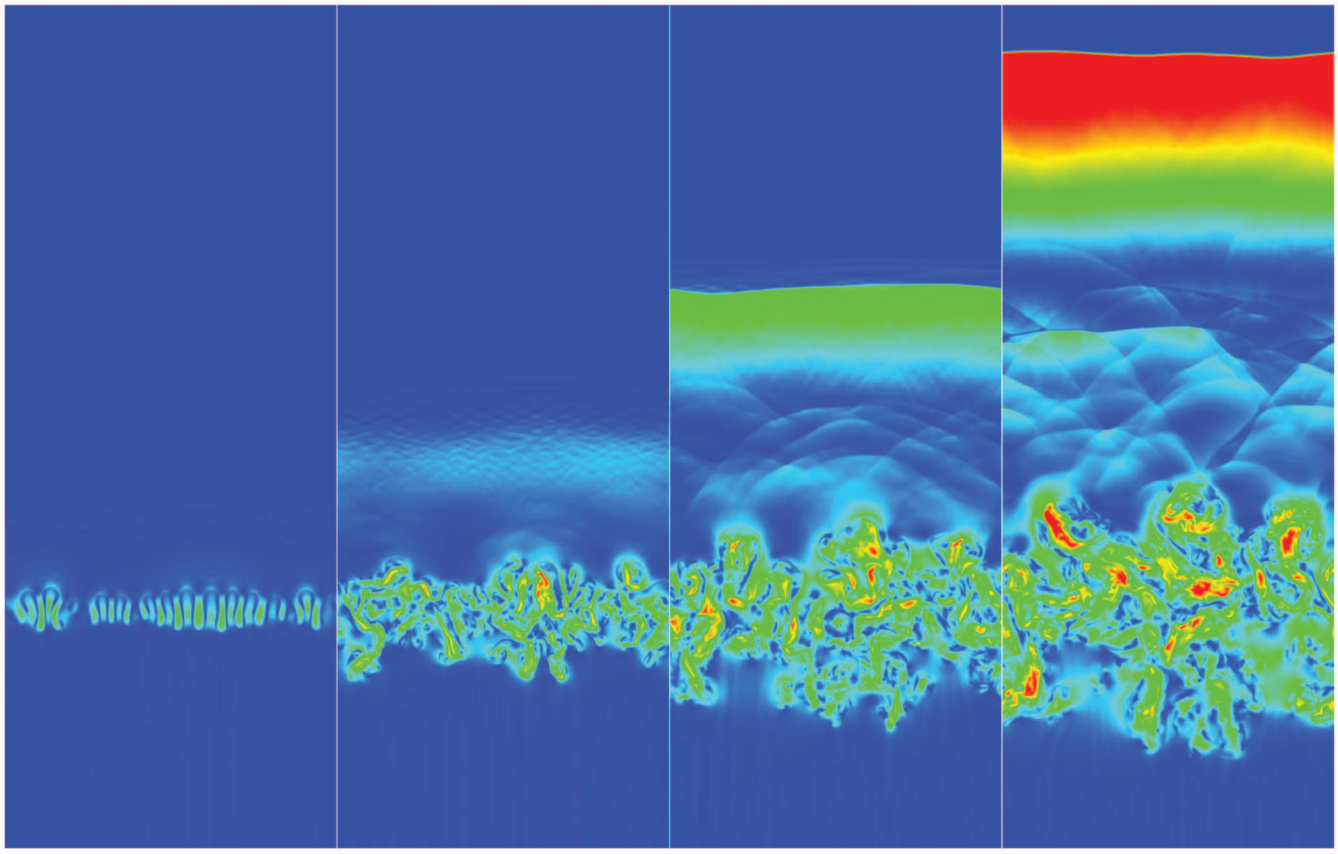

FIG. 1. (Color) Local Mach number from a 512×2048 point simulation of compressible R-T instability. The upper fluid is xenon and the lower fluid is neon. The RGB color map ranges from 0 (blue) to 1 (red). The snapshots show a 12.8×32.6 km portion of the 12.8×51.2 km flow domain. Simulation times from left to right are: $t=25$, 50, 75, and 100 s.

ber in the mixing region and distinct shocklets fill the region between the mixing layer and the main shock. The neon bubbles appear to act like pistons, sending compression waves into the xenon, which catch up to previous waves, thus reinforcing the shocklets. The shocklets then combine multidimensionally with their neighbors to form the main shock. This process is driven, in part, by expansion of the bubbles of light fluid as they rise in altitude. The phenomenon bears some resemblance to a deflagration-to-detonation transition (DDT), where acoustic waves emanating from the combustion front combine in multidimensional fashion to form a shock.[12]

Figure 2 shows flow features from a corresponding 3D simulation at a time well after the main shock has formed. The shock wave increases in Mach number as it propagates down the hydrostatic density gradient. A shock does not form in the lower fluid because density increases at lower elevations, i.e., momentum conservation dictates that velocity must decrease as density increases and vice versa.

In constructing a model of the shock formation process, we can make direct use of the piston analogy. Consider the canonical compression wave problem wherein a piston in a 1D tube is given a constant acceleration, a.[13] The acceleration may be thought of as a series of infinitesimal velocity jumps, which produce finite compression waves emanating from the piston surface. The first wave originates from the piston at $t=0$ and travels at the speed of sound in the undisturbed fluid, c_0. The second wave originates at $t=dt$ and travels at c_1+du, where c_1 is the sound speed behind the first wave and du is the piston velocity after the first jump. Simple compression waves satisfy the jump relation,[14]

$$u_1 - \frac{2}{\gamma-1}c_1 = u_0 - \frac{2}{\gamma-1}c_0, \tag{5}$$

which for the present case reduces to $c_1=c_0+(\gamma-1)du/2$. The distance at which the second wave overtakes the first wave is

$$L_p = \frac{2c_0^2}{a(\gamma+1)}, \tag{6}$$

where $a=du/dt$. This distance to intersection of the characteristics corresponds to the location where the shock begins to form.

The relevant acceleration for R-T instability, which appears both in linear stability theory[15] and in the similarity equation for the late-time growth rate,[16,17] is Ag, where $A\equiv(W_2-W_1)/(W_2+W_1)$ is the Atwood number for ideal gases (with W_1 and W_2 are the molecular weights of the light and heavy gases, respectively). Setting $a=Ag$ in Eq. (6) yields

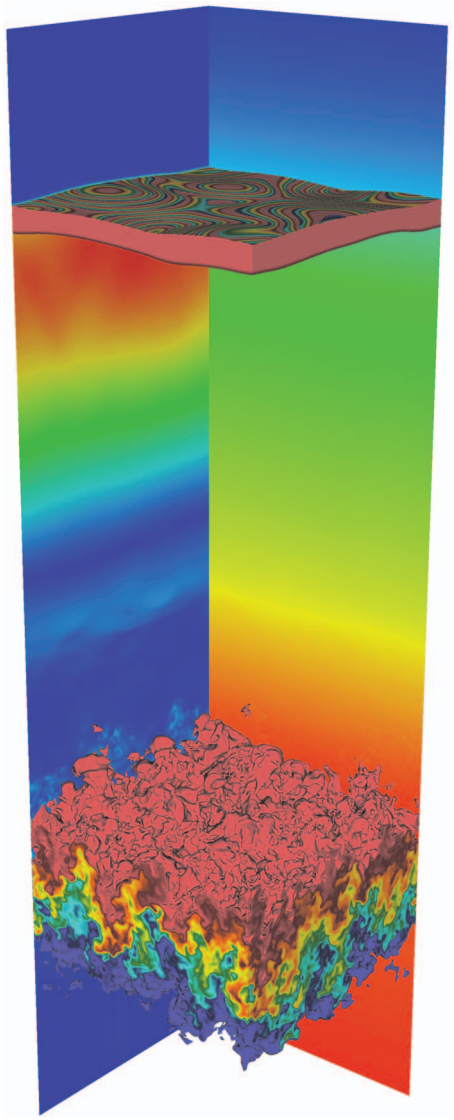

FIG. 2. (Color) Three-dimensional ($256\times256\times1024$) simulation of xenon over neon in a $12.8\times12.8\times51.2$ km domain at $t=105$ s. The lower isovolume shows the xenon mass fraction in the range 0.1–0.9. The upper isovolume is temperature in the range 3000–4400 K, with a color map ranging from 1700 to 3300 K. The left back plane is the local Mach number, where 0 is blue and 1.978 is red. The right back plane is density on a log scale, covering the range $0.005264-1.680\times10^{6}$ g/cm^3.

$$L_s = \frac{2c^2}{Ag(\gamma+1)} \tag{7}$$

as the relevant length scale for R-T shocks, where c is the sound speed in the upper fluid.

In order to test whether Eq. (7) is an effective gauge of the shock formation height, we conducted a set of 3D simulations using Atwood numbers of 0.221, 0.533, and 0.734. These Atwood numbers correspond, respectively, to krypton, argon, and neon as the light fluid. All three simulations were performed by discretizing a 12.8 km$\times$12.8 km$\times$51.1 km domain into $128\times128\times512$ grid cells. The Gaussian perturbation spectrum applied in each simulation was centered about mode number 16. The fluid interface was placed one quarter of the distance from the bottom boundary to the top boundary in order to allow sufficient room for the shock to form in the xenon. Except for the lower fluid, the simulations were all identical. In conjunction with the 3D simulations, we performed a corresponding set of 2D simulations (same perturbations and fluids, etc.) in order to assess the effects of dimensionality on the shock formation process.

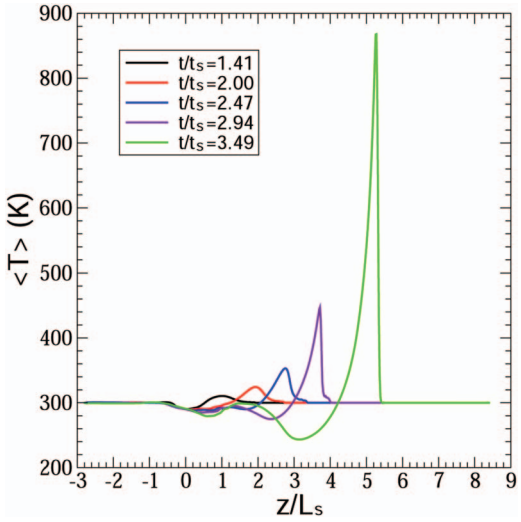

FIG. 3. (Color) Temperature profile at various times for the 3D argon case.

We define the shock location, z_s, as the z location where $\langle T\rangle$ reaches its maximum. Here we use angle brackets to denote a horizontal (x,y) average. Figure 3 displays profiles of $\langle T\rangle$ from the 3D argon simulation at three different nondimensional times, where $t_s \equiv c/Ag$. The temperature profiles indicate that the main shock forms in the region $1<z/L_s<3$ and then rapidly increases in strength as it propagates down the hydrostatic density gradient. The Mach number of the shock, M_s, is evaluated from the temperature jump condition

$$\frac{\langle T\rangle_{\max}}{T_o} = \left[1+\frac{2\gamma}{\gamma+1}(M_s^2-1)\right]\left[\frac{2+(\gamma-1)M_s^2}{(\gamma+1)M_s^2}\right]. \tag{8}$$

This jump condition provides an unambiguous measure of the average strength and location of the shock, since T is initially constant. The shock Mach number versus shock location is plotted in Fig. 4 for all six simulations. In every case, $M_s\to1$ as $z_s\to L_s$; hence, the main shock waves all begin to form at approximately a distance L_s above the fluid interface. It is also apparent that the argon and neon simulations produce similar shocks, whereas the krypton case produces a somewhat weaker shock. Additional tests (not shown) indicate that better collapse of the Mach number curves is obtained at higher Atwood numbers. It is noteworthy that the 2D simulations all produce weaker shocks than their 3D counterparts. This may be a result of increased interaction among the shocklets in 3D compared to 2D, or it may be due to differences in 2D and 3D growth rates of the mixing layer.[18]

Given the robust manner in which R-T instability produces shock waves, it is natural to ask why this phenomenon was not observed in earlier studies. In order to answer this question, consider the turbulent Mach number as defined by Mellado *et al.*,[9] $M_t(z,t)\equiv\langle\|\mathbf{u}\|\rangle/\langle c\rangle$. This Mach number is plotted versus height in Fig. 5 at several different times for

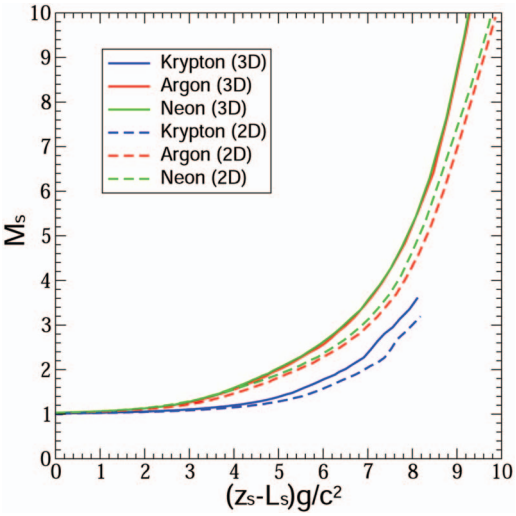

FIG. 4. (Color) Shock Mach number as a function of shock location. The abscissa is the nondimensional distance between the shock (z_s) and its expected height of formation (L_s). The curves depict a temporal evolution of the flow, i.e., $z_s=z_s(t)$.

the 3D argon case. The Atwood number for this case ($A=0.533$) is close to the $A=0.5$ simulations of Mellado *et al.* Mellado *et al.* used $M_t(0,t)$ as a gauge of compressibility effects. In their simulations, the distance from the fluid interface to the top boundary of the domain was $2.825L_s$. From Fig. 5 it is apparent that this distance is too short to capture the true maximum of M_t. The turbulent Mach number at $z=0$ appears to reach a constant maximum of approximately 0.2; however, by $t\approx 2.2t_s$, M_t just behind the main shock has overtaken $M_t(0,t)$; hence, $M_t(0,t)$ is not a reliable indicator of compressibility effects at a late time.

Finally, the present results raise the question as to whether R-T shock waves could provide a detonation mechanism for type Ia supernovae. Relevant parameters for an exploding white dwarf are $c\approx 7\times 10^8$ cm/s, $g\approx 10^{10}$ cm/s^2, $A\approx 0.25$, and $\gamma\approx 4/3$; hence, a rough estimate of the shock formation length is $L_s\approx 1700$ km. This is fairly close to the ~2500 km radius of the expanded star, which leaves some doubt as to whether the shock would have sufficient space to form. Our scoping studies using a Helmholtz equation of state[19] have thus far failed to produce a shock of sufficient strength to ignite the carbon.[20–22] However, it may be possible that hydrodynamic expansion of rising bubbles, augmented by thermonuclear expansion, results in faster shock formation. Further studies are needed to investigate this hypothetical synergy between buoyancy and heat release.

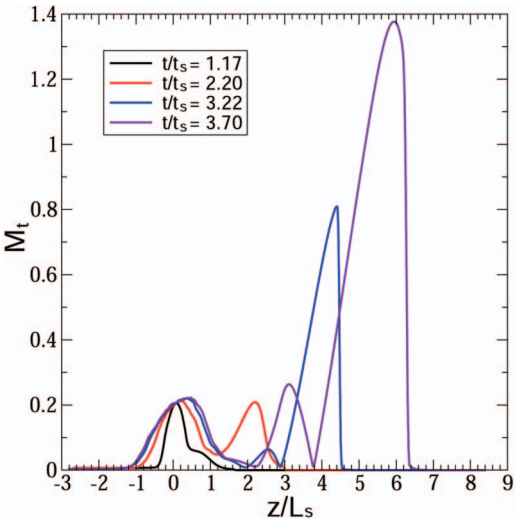

FIG. 5. (Color) Turbulent Mach number vs height for the 3D argon case. For each curve, the bulge around $z/L_s=0$ corresponds to the mixing layer. The larger bulges to the right correspond to shocks and rarefactions in the upper fluid.

We are grateful to Dr. W. H. Cabot for help in writing the code. This work was performed under the auspices of the U.S. Department of Energy by the University of California Lawrence Livermore National Laboratory under Contract No. W-7405-Eng-48.

[1] F. X. Timmes, "On the acceleration of nuclear flame fronts in white dwarfs," Astrophys. J. Lett. **423**, L131 (1994).
[2] K. Nomoto, K. Iwamoto, and N. Kishimoto, "Type Ia supernovae: Their origin and possible applications in cosmology," Science **276**, 1378 (1997).
[3] E. J. Lentz, E. Baron, and D. Branch, "Sn 1984a and delayed-detonation models for type Ia supernovae," Astrophys. J. **547**, 402 (2001).
[4] V. N. Gamezo, A. M. Khokhlov, and E. S. Oran, "Three-dimensional delayed-detonation model of type Ia supernovae," Astrophys. J. **623**, 337 (2005).
[5] M. Zingale, S. E. Woosley, C. A. Rendleman, M. S. Day, and J. B. Bell, "Three-dimensional numerical simulations of Rayleigh–Taylor unstable flames in type Ia supernovae," Astrophys. J. **632**, 1021 (2005).
[6] F. K. Röpke and J. C. Niemeyer, "Delayed detonations in full-star models of type Ia supernova explosions," Astron. Astrophys. **464**, 683 (2007).
[7] J. Zhang, O. E. B. Messer, A. M. Khokhlov, and T. Plewa, "On the evolution of thermonuclear flames on large scales," Astrophys. J. **656**, 347 (2007).
[8] M. Zingale and L. J. Dursi, "Propagation of the first flames in type Ia supernovae," Astrophys. J. **656**, 333 (2007).
[9] J. P. Mellado, S. Sarkar, and Y. Zhou, "Large-eddy simulation of Rayleigh–Taylor turbulence with compressible miscible fluids," Phys. Fluids **17**, 076101 (2005).
[10] A. W. Cook, "Artificial fluid properties for large-eddy simulation of compressible turbulent mixing," Phys. Fluids **19**, 055103 (2007).
[11] A. W. Cook and P. E. Dimotakis, "Transition stages of Rayleigh–Taylor instability between miscible fluids," J. Fluid Mech. **443**, 69 (2001).
[12] E. S. Oran and V. N. Gamezo, "Origins of the deflagration-to-detonation transition in gas-phase combustion," Combust. Flame **148**, 4 (2007).
[13] J. D. Anderson, *Modern Compressible Flow* (McGraw-Hill, New York, 2004.
[14] R. Courant and K. O. Friedrichs, *Supersonic Flow and Shock Waves* (Interscience, New York, 1948).
[15] S. Chandrasekhar, *Hydrodynamic and Hydromagnetic Stability* (Oxford University Press, Oxford, 1961).
[16] J. R. Ristorcelli and T. T. Clark, "Rayleigh–Taylor turbulence: Self-similar analysis and direct numerical simulations," J. Fluid Mech. **507**, 213 (2004).
[17] A. W. Cook, W. Cabot, and P. L. Miller, "The mixing transition in Rayleigh–Taylor instability," J. Fluid Mech. **511**, 333 (2004).
[18] W. Cabot, "Comparison of two- and three-dimensional simulations of miscible Rayleigh–Taylor instability," Phys. Fluids **18**, 045101 (2006).
[19] F. X. Timmes and F. D. Swesty, "The accuracy, consistency, and speed of an electron-positron equation of state based on table interpolation of the Helmholtz free energy," Astrophys. J., Suppl. Ser. **126**, 501 (2000).
[20] F. X. Timmes and S. E. Woosley, "The conductive propagation of nuclear flames. I. Degenerate C+O and O+Ne+Mg white dwarfs," Astrophys. J. **396**, 649 (1992).
[21] S. E. Woosley, S. Wunsch, and M. Kuhlen, "Carbon ignition in type Ia supernovae: An analytic model," Astrophys. J. **607**, 921 (2004).
[22] T. Plewa, A. C. Calder, and D. Q. Lamb, "Type Ia supernova explosion: Gravitationally confined detonation," Astrophys. J. Lett. **612**, L37 (2004).